Paleo-earthquake Evidence and Earthquake Recurrence for Düzce Fault, Turkey

Tolga Komut (tolga.komut@gmail.com)
Çanakkale Onsekiz Mart Üniversitesi https://orcid.org/0000-0003-1248-9811
Ersin Karabudak
Boğaziçi University

Manuscript

Keywords: paleoseismology, North Anatolian fault, Düzce fault, 1999 Düzce earthquake

Posted Date: January 30th, 2021

DOI: https://doi.org/10.21203/rs.3.rs-173382/v1

Version of Record: A version of this preprint was published at Journal of Seismology on March 25th, 2021. See the published version at https://doi.org/10.1007/s10950-021-10002-7.

Abstract

Paleoseismological trenching was performed along the Düzce fault providing some preliminary insight about its seismogenic behavior. Dating was based on radiocarbon analysis of peat samples collected from the trenches and suggested seven earthquakes have occurred since 1740 BC. Integrating date constraints of events exposed in the trenches suggests a periodical earthquake recurrence model. According to a linear sequential event serial that has minimum misfit determined by considering the probability curve limits of the sample dates, the earthquake recurrence interval is between 384 and 460 years (or possibly between AD 394 and 400). A probability curve was also calculated for the date of the last earthquake (1999 Düzce earthquake) considering the probability distributions of sample dates based on the same event serial. This probability-distribution-based method, similarly, predicted that the 1999 Düzce earthquake occurred between 1933–2005 (± 36 years) with a 68 % probability. After this verification. Using this method, it was estimated that the next earthquake along the Düzce fault has a 68 % probability of occurring between 2328–2392. According to this calculation, the earthquake recurrence interval is about 391 ± 34 years with a 68 % probability and the AD 967 historical earthquake likely ruptured the Düzce fault. Assuming an average slip of 350 cm (the average slip of the 1999 earthquake), the slip rate was estimated to be between 8.7–11.2 mm/a.

1. Introduction

On November 12, 1999, a destructive earthquake struck the town of Düzce (Turkey), resulting in tragic deaths and considerable structural damage to buildings. The ruptured Düzce fault is part of a branch of the North Anatolia fault (NAF) that extends along the southern border of the Düzce basin (Fig. 1). The earthquake produced about 42-km of dextral rupture with 350-cm average slip (Fig. 2). This right lateral fault is likely composed of four segments (Efteni, Aydınpınar, Mengencik and Kaynaşlı), each having similar length, and are separated by left-stepping structural discontinuities (stepovers) that result in pressure ridges (Fig. 3a). Previous paleoseismic studies suggest that the fault is a single segment (Hitchcock et al. 2003; Emre et al. 2002, 2004; Pantosti et al., 2008).

Three historical earthquakes in **AD 1719, AD 1509** and **AD 967** likely originated from the Düzce fault. According to Ambraseys and Finkel (1995), a destructive earthquake struck the Düzce area on May 25, **1719** (also Konukçu 1984) and was like the 1999 Kocaeli rupture. The AD 1509 earthquake, occurring on September 10, is well known as “the great **1509** historical İstanbul earthquake”, and may have extended the entirety of the Düzce basin. Finally, the oldest earthquake, dating back to September 2, **967** has limited recorded information from Claudiopolis (present day Bolu) and Constantinople (present day İstanbul) (Bakır 2002; Ambraseys and Jackson 1998). While the earthquake was substantial in Claudiopolis, there was no damage in İstanbul (Bakır 2002). However, there have been no studies with any information about the effect of this earthquake in the Düzce area probably because Düzce has a relatively new residential area.

The object of the current paleoseismic trenching study is to provide constraints for the dates of past earthquakes that ruptured the Düzce fault. Eleven paleoseismic trenches were excavated in three sites (Fig. 3b) along the Aydınpınar and Mengencik probable segments. Five trenches that crosscut the 1999 rupture contain a variety of seismological traces (stratigraphic and structural evidence) suggesting six earthquakes occurred since 1750 BC that predate the 1999 event. Seven 14C accelerator mass spectrometry (AMS) dates were used to obtain preliminary information about the recurrence intervals for large earthquakes originating from the Düzce fault. According to a sequential earthquake serial set suggested in this study, the recurrence interval is between 394 and 400 years based on the limit values of pre- and post-dating samples, respectively. On the other hand, the recurrence interval was estimated to be about 391 ± 34 years with a 68 % probability based on a probability distribution of dates of the seven samples. The results here will be helpful for addressing questions such as: 1) Is it the character of Düzce fault that typically results in a rupture as a single segment? or are there multiple segments along the Düzce fault that can fail individually? 2) If the Düzce fault is a single segment, does it produce characteristic earthquakes? and 3) Did the surface ruptures of the **1719, 1509**, and **967** historical earthquakes occur along the Düzce fault?

2. Site Description And Trench Locations

The Düzce fault, that extends along the southern border on the Düzce plain, and transverses Quaternary alluvial fans, were built by northward-flowing streams. The fans are composed mostly of alluvium derived from sandstone rocks from the mountain side that were carried by the drainage system. Unstratified gravel deposits of alluvial fans are also common. They were derived from the mountain front in flooding periods and are interfingered with massive clay deposits having a low energetic environment on the plain. Paleoseismic data were collected from three sites along the Mengencik and Aydınpınar probable segments. The Töngelli and Bend sites are on the Mengencik segment and Kaledibi site is on the Aydınpınar segment. Eight trenches were excavated on the Mengencik segment (Figs. 3 and 4). Three of the trenches were exploratory (Çayır-1, Çayır-2, Bend-2) and five (Töngelli-1, 2, 3; Bend-1, 3) were main trenches. For the Kaledibi site, three trenches were excavated along the eastern part of the Aydınpınar segment (Fig. 3). Two of them were exploratory (Kaledibi-2,3) and the other one was the main trench (Kaledibi-1).

The surficial expression of the Düzce fault consists of a prominent set of linear shutter ridges (Mengencik and Kahveci ridges) along the Mengencik segment (Fig. 4). The Çayır, Töngelli and Bend streams that flow northward from the mountain front are the primary sources of young sediment for the trench sites along this segment. South of the shutter ridges, fault ruptures were probably buried by late-Holocene deposits from these streams. Töngelli-1, 2, and 3 and Çayır-1 and 2 trenches were excavated in the Töngelli site in the year following the 1999 earthquake (Fig. 4). The dextral displacement from the surface rupture of the 1999 Düzce earthquake in the Töngelli-1 trench location was 450 cm. The Töngelli stream is small and dry, especially in the summer, and feeds a small alluvial fan (Fig. 5). There is a smaller alluvial fan to the east that belongs to the Çayır stream, about 10 m east of the Töngelli fan. It crosses the rupture zone like the Töngelli fan. The fan has a very low energetic sedimentary environment. Two

exploratory trenches (Çayır-1 and − 2) were excavated at this site (Figs. 4 and 5) that have uniform sedimentation. On the other hand, Töngelli-1 trench was excavated on the Töngelli stream fan which represents a relatively higher energetic environment. To the west of the Töngell-1 trench, there is a narrow valley parallel to the fault between the mountain front and the Mengencik shutter ridge in the Töngelli site (Fig. 4). The 1999 rupture formed a narrow (a few meters wide) long trough along this valley (Fig. 6). Two trenches (Töngelli-2, 3) were excavated across the fault zone in this valley (Fig. 5).

In the Bend site along the Mengencik segment, Bend-1, 2, and 3 trenches were excavated in the 2nd year after the 1999 earthquake. The juxtaposition of the Kahveci shutter ridge, on the north side of the fault, against the Bend stream valley, on the south side, results in blockage of the Bend stream drainage and its alluvial fan (Figs. 4 and 7). Excessively accumulated alluvium from the blocked drainage appears to result in a westward-propagating alluvial fan (Fig. 4). The drainage is channelized to the west, through the gate between Mengencik and Kahveci shutter ridges. This deflection of the stream caused by accumulated right lateral slip along the Düzce fault also results in formation of the shutter ridges. Massive clay and flood deposits from the Kahveci ridge site dominate the trench exposures at the site.

Two years after the 1999 earthquake, Kaledibi-1, 2, and 3 trenches were excavated near the west of Kaledibi village in the Kaledibi site along the Aydınpınar segment (Fig. 8). The 1999 surface rupture consisted of approximately 15 cm southside-down vertical and 350 cm of right-lateral offset in the excavated area. In this site, there is a small stream that flows northward from the mountain front to the Düzce plain. Its channel slightly turns east where it juxtaposes against the northeastern extension of a small topographic rise (a shutter ridge between 31˚09′40″ and 31˚09′50″ longitudes) to the north. There is a south facing scarp of the Düzce fault along the southern slope of the topographic high, several meters north of the stream. The height of the south facing fault scarp varies between 60–90 cm. Since this is up to 6 times higher than the scarp that was formed by the 1999 Düzce earthquake, it is reasonable to suspect that the scarp was formed by multiple prior ruptures.

3. Trench Exposures

Low energetic and continuous sedimentation environments that provide good stratigraphic resolution could not be selected. Although stratigraphy is continuous in low energy domains, its contrast is too low along the Düzce fault (e.g., Çayır-1, see Fig. 5). To overcome this problem, the trenches were purposely located in depositional environments that likely had relatively higher sedimentation. For this reason, the trench locations were chosen near the mouths of small-to medium-size drainage valleys where the grain size is predominantly sand and pebbles. This strategy increased the visibility of the paleoseismic indicators within the stratigraphy. Shallow groundwater-levels were another problem in this field that only allowed excavation to limited depths (2–4 m), even though the trenches were excavated in late-summer or autumn. Strong flooding events also made it impossible to find more than one or two events in the trenches. Although the stratigraphy in the trenches has poor contrast because sediments are not thinly bedded, sharp contrasts that allow faulted and un-faulted units to be differentiated from each other were present within the trench exposures. In many cases, fissures filled with massive clay deposits provided

pre- and post-dates for dating earthquake horizons. Horizontal and vertical grids were formed with squares using string to serve as a reference frame for logging trench walls. Logging scales ranged from 1:10 to 1:20. Most of the trenches were documented by detailed drawings (trench logs) at a scale of 1:10. Log scale and grid size depended both on the complexity of exposure and stability of the trench walls. Small scales had to be used when the trench walls seemed too unstable (e.g., Kaledibi-1 trench).

Seven radiometric ages (AMS) of samples were dated and calibrated (Bronk Ramsey 1995, 2001, 2004) to the RAFTER Radiocarbon Laboratory, Institute of Geological and Nuclear Sciences in this study. Calibration of the reported conventional radiocarbon ages were made based on atmospheric data from Stuvier et al. (1998). The calendar ages of the samples are between 1750 BC and AD 1950 with a 95 % probability. Because the calibration curve is not monotonic, possibility ranges of some of the radiocarbon ages intercept the curve at more than one location. This resulted in more than one possible calibrated date range for some samples. The sample information, date ranges with possibility, and corresponding events were given in Table 1. Three sampled units are younger (post-date) and four are older (pre-date) than the event horizons.

3.1. Töngelli-1

The alluvial fan of the Töngelli stream in the Töngelli site (Fig. 4) was excavated perpendicular to the surface rupture of the 1999 earthquake (Fig. 5) in late summer. The eastern wall of the North-South trending 15-meter-long trench, which cuts the 1999 surface rupture, was mapped at a scale of 1:10 (Fig. 9). The excavated trench exposed predominantly silty clay and gravelly strata that was divided into two structural blocks separated by a fault zone around the 5.5th meter of the trench. Since there was a high groundwater level, and therefore, high risk of wall collapse, only the upper 2 m of the trench was examined. Based on the best data that could be collected from this trench considering these difficulties, at least two conspicuous faulting events occurred before the 1999 Düzce earthquake. The oldest event (**event A**) was recognized as a dropped blog (local normal faulting) between the 8th and 10th meters (Fig. 9). The other event (**event F)** observed in the exposure was thought to be related to this compressional structure. A sediment-fill that post-dates **event F** was deposited between 0–4 meters on the southern flank of the structure (Fig. 9). Strata in the excavation are coded with letters from A to G (Fig. 9). Some brick pieces were collected in units B and G. The gravelly units (B and E) indicate that floods sometimes buried alluvium. A sample (R26946/1 in Table 1) that pre-dates the gravelly unit B suggested at least one flood in the past 3500 years. Several finer grained gravelly layers in unit B display flow structures indicating that the sedimentation rate was likely very high during flooding periods. The thickness of the poorly sorted gravel deposits varies from unit to unit. Silty clay units represent low energetic environments (units D, C, F) between the flooding events. Greenish C and F units, and the upper parts of D unit have massive silty clay deposits. In contrast, the stratigraphy in unit A predominantly consists of well-bedded sandy and silty sediments that are less than about 600 years old according to a predating sample of R26946/4 (Table 1).

The G unit has a chaotic structure and represents the deformation zone, that is, the fault zone (Fig. 9). For this reason, it was difficult to differentiate **event F** from the 1999 earthquake. Although a precisely located 1.5 m wide deformation zone on the surface rupture was very clear, cracks from the 1999 rupture were not visible in the trench. The deformation zone (around the 5.5th meter), that probably contains more than one event, was too indecipherable to allow events to be distinguished. The units on both sides of the deformation zone that separates the trench into two structural blocks are bent towards the surface (upwards) along this deformation zone. A sediment-fill, that post-dates **event F**, was deposited on the southern flank (between 0–4 meters) of this compressional structure. The sagging seems to have occurred between the push up structure in the north and the slope of the hill to the south. The primary position of sediments in unit A was unchanged, meaning the sedimentary layers of well-bedded unit A in the northern side of the trench is not deformed. The structure was thought to be caused by compression related to a push-up structure of a mole track. This structure may also be related to local irregularities of the strike (e.g., left bending) during dextral faulting. However, at the trench location, no significant slope was observed that was related to the last rupture (1999 event). The lateral offset of the 1999 surface rupture is about 450 cm in this location. The deposition likely developed in a local sag (around the 5.5th meter) that was formed between the southern flank of the compressional structure and the slope of the mountain to the south. The sag shape of the paleo-surface that appeared during **event F** remained virtually intact and uneroded. It was buried then preserved under horizontal layers of unit A. Well-laminated silty sands with silty clays (unit A) fill the upper parts of the sag. Some gravel shortly fill the bottom tip of this structure after its formation. The date of **event F** when a depression formed is constrained by two accelerator mass spectrometry (AMS) radiocarbon ages (Fig. 9), which are listed in Table 1. Based on the dating of two samples of peat, unit A is consistently younger than unit D, confirming the stratigraphic order in the exposure. The sedimentation date of the gravel in unit A, located at the bottom tip of the depression, is in the range of AD 1520 and 1800 according to a 68.2 % probability curve for the age of sample R 26946/5. On the other hand, the upper part of unit D was deposited between AD 1400 and 1460 with 68.2 % probability according to the age of sample R 26946/4. This range that pre-dates **event F** represents the younger part of unit D. According to these data, the preferred date of **event F** is between AD 1400 and 1600. However, ages as old as 1310 and as young as 1950 are also possible, but with lower probabilities according to calibrated dates of samples (Table 1).

The vertical separation of unit E, which can be ascribed to another seismic event, appears near the northern part of the Töngelli-1 trench (Fig. 9). This event was referred to as "**event A**" in this study. A set of two faults (fault "a" and "b") terminate upward in the massive silty clay deposits of unit C and form a depressional structure. An apparent vertical offset of 30 cm occurred between these faults during **event A**. This dropped blog structure, between the faults that have normal components (Fig. 9), shows similarity in both size and shape to the trough structure caused by the 1999 surface rupture in the Töngelli-3 trench (Fig. 6). These normal faults are inferred to have a dextral component, although not noticeable from the trench wall. Over 100 cm of the 20-cm-thick gravel unit E is displaced downward by these faults between the stations at the 8th and 10th meters of the exposure. Its upper and lower surfaces are displaced by the same faulting geometry and amount (30 cm). The faulting occurred prior to gravel deposition of flood

unit B because its lower surface was not affected by faulting. At the upper part of unit C that has massive nature, scarps, and the depression, if any, were completely undetectable. The invisible upper edges of the faults (a and b) in unit C should have been overlain by the upper part of the unit because debris or remains of the gravel of unit E were not observed along the fault and the overhanging scarp did not collapse. However, the event horizon could not be identified in unit C because faults could not be followed in the massive clay area of the unit. Thus, it is not clear whether the faults were formed just before the deposition of unit B or just after the deposition of unit E. However, it is quite clear that these faults were not reactivated after the deposition of unit B. This is proven by the intact sediments of unit B that blanket the fault. One dated sample of peat near the top of unit E, on the up-thrown side of fault “a” (Fig. 9), indicates that a flood bed was deposited around the middle of the millennium before the last millennium BC and it post-dates unit E. The sample, about 1.6 m below the ground surface, yielded accelerator mass spectrometry (AMS) of radiocarbon date ranges between 1740 − 1530 BC according to a less probable part of the 68.2 % probability region of the probability curve for age. It ranges from 1700 − 1600 BC according to a more probable part of the 68.2 % probability region (Table 1, sample R26946/1). The date of the faulting event, leading to the formation of a depression between faults “a” and “b”, is represented by this radiocarbon date. This sample pre-dates **event A** and post-dates unit E suggesting that faulting occurred after 1740 BC.

3.2. Töngelli-3

The Töngelli-3 paleoseismic trench was excavated across a small east-west trending valley, between the Mengencik shutter ridge and the northern slope of the Almacık Mountain. It cut the surface rupture of the 1999 Düzce earthquake perpendicularly (Figs. 4 and 5) that has about 450 cm dextral offset in this area. In the trench location, the rupture exhibits a trough geometry having a ~ 50 cm depth (Fig. 6). Although the trench was excavated in mid-autumn, when the groundwater-table-level was expected to be low, the site actually had a high groundwater-table, which caused difficulty during trenching. The exposure was mapped at a relatively small scale (1:20) because the trench had high risk of collapse despite firm arbitration. The exposed stratigraphy generally consists of silty clay and gravel (Fig. 10). A massive silty clay layer that existed almost the entire length of the trench was an undifferentiated package (unit A). The top surface of the gravel unit (unit B) in the bottom of the trench gently sloped? down to the center of the valley. There was also trash covering the units that was thrown from a nearby exploratory trench excavation (of Töngelli-2) before the Töngelli-3 trench was explored. The decision to open the Töngelli-3 trench was made after excavating the Töngelli-2 trench that was at a lower topographic level. Because Töngelli-2 had a very high groundwater table, it was unstable and too risky, to be mapped. In fact, most of the walls collapsed during the excavation. There was also limited time to explore the walls of Töngelli-3 trench, but we managed to complete limited observations.

Two events were recognized in the trench other than the 1999 rupture. Two fills (Fig. 10, 1st-2nd and around 5th meters) of depressions formed by the steep scarps of the fault zones, along the deformation zone of the 1999 rupture is evidence of these events. In addition, the most prominent marker bed was unit B in the exposure faulted by these two events (Fig. 10). These events, around 1.75 m and 5 m, were distinguished by the two fissure-fills, called unit C and unit D, respectively, in a massive silty clay unit (unit

A). Therefore, unit A must have been faulted by these events. However, the faults are invisible because of massive nature of the silty clay deposition (unit A). The depressional structure of the 1999 event observed on the surface (Fig. 6) and in the trench are similar in size and geometry to what was suggested for the fissure-fills here (Fig. 10). The depressions (i.e., fissures and its fills related to these events), are continuous along the valley as observed in the fracture of the 1999 event because during the excavation and collapse of the parallel exploratory trench (Töngelli-2), the positions of both were observed to be compatible with fault strike. The trough-like morphology of the site is related to the eastward movement of the shutter ridges along the fault zone with respect to the main slope of the hill. Upper surfaces of unit C and D fills indicate the levels of the horizons. The event in the lower parts of the trench to the north, and distinguished by unit D, could not be dated because unit D and unit B have similar material and intersect.

Besides the 1999 earthquake, the youngest event recognized in the Töngelli-3 trench (Fig. 10, from the southern wall to 3rd meters) is referred to as **event E**. The depressional trough, formed in the horizon at that time, was filled with gravelly sands of unit C and then covered by upper levels of unit A. The fault tips at the 0- and 3-meters stations terminate at the same stratigraphic level, which lies between 40 and 50 cm below the ground surface. After the massive flood deposition of unit B, silty clay material of unit A was uniformly deposited in a low energetic environment. At the time of **event E**, the silty clay deposition was locally interrupted. The pleo-earthquake caused sets of normal faulting both in unit A and unit B and post-date them. The resultant fissure on the event horizon in unit A was filled by gravelly sands (unit C). A peat sample (R28325/10) collected from the base of unit C post-dates **event E** (Fig. 10). The sample's AMS 14C age ranges from AD 1230 to 1290 (Table 1). Therefore, **event E** occurred before AD 1290.

3.3. Bend-1

Bend-1 trench was excavated in late-summer at the Bend site and is perpendicular to the 1999 surface rupture (Fig. 7), which has about 450 cm dextral offset here. The sediments of the Bend-1 trench are massive clays, silts, and gravels (Fig. 11). Massive clay sediments of unit A and C and flood deposits of unit B originated from the Kahveci ridge based on the thickness variation and surface slope of the trench site. On the other hand, the slope of unit B in the opposite direction (i.e., towards the north), is probably related to structural deformations from the paleo-earthquakes. Detailed mapping of the trench wall is lacking because of poor logistical conditions and very high collapse risk. However, detailed mapping was not necessary for this exposure because there was simple stratigraphy in the trench. The 1999 surface rupture is 1 m north from the northern boundary of the logged section. There was evidence of a single event with a gravelly fissure-fill (unit D), recognized in the trench exposure (between 1st and 2nd meters) and located 2.5 meters south of the 1999 rupture. This event was referred to as **event C**.

Unit A has massive silty and clay deposits (i.e., invisible stratigraphy to allow to distinguish the faults). However, the upper surface of unit D is considered the event horizon, and a marker that distinguishes both the parts of unit A and possible position of the faults accumulated before and after **event C**. It is a local and discontinuous structure called a tension crack that was not seen in the Bend-2 trench that is parallel to the Bend 1 trench, 10 meters away (Fig. 7a). This was important evidence to conclude that the structure is not a flow channel but may be a fissure structure. In addition, Bend stream, 200 meters ahead,

flows westward beyond the trench area. However, it is perplexing that there was no observable thickness change in unit B that would indicate lateral slip along the dextral fault zone (Fig. 11), because parts of different thicknesses of the unit were not juxtaposed by the lateral fault. The most likely reason for this is the uniform thickness and flat state of unit B along the fault direction as observed by the pebbles spread over the current surface in the close vicinity. Based on the stratigraphic position of the gravel-fill (unit D), two fault strands that are connected in unit C, cut gravelly unit B and unit C, terminate upward into the lower massive clay deposits of unit A, and produce about a 50-cm- deep depression in the lower parts of unit A. Units D and A probably completely buried evidence of deformation, including the fissure structure produced by **event C**. Faults attributable to **event C** are probably normal and were generated by a tension crack (T fracture) of mole track. The current topography is a south-dipping plane that does not reflect the irregular topography produced by the event beneath the depression. It is likely that the depression was left almost intact and unopened until it was protected by unit D. It is probable that the event horizon lies along the upper boundary of unit D. A peat sample (R28325/9) just below the expected event horizon (Fig. 11) yielded an accelerator mass spectrometry (AMS) calibrated radiocarbon date of AD 440–540 (Table 1). This result indicates that **event C** likely occurred after about AD 440.

3.4. Bend-3

This trench consisted of a perpendicular cut to the 1999 Düzce earthquake surface rupture. It was excavated parallel to the Bend-1 and Bend-2 trenches about 200 m to the east (Fig. 7) in late-summer. Gravel and silty clay deposits were exposed in the trench (Fig. 12), and unit C extends its entire length. It is an unstratified (massive) silty clay deposit that causes great difficulty in recognizing cracks related to paleo-earthquakes, even the 1999 rupture (Fig. 12). A poorly sorted gravel bed was thought to have been derived from the mountain front (south) during a recent flood in Bend stream (Fig. 7). Flood deposits could be separated into two units. These are a weakly consolidated fine-sand layer of unit B and an overlying pebbly unit A. The 1999 event right laterally shuttered and offset the northern extension of the flood deposits (unit A and B) about 450 cm to the east.

About a meter to the north of the 1999 surface break, a wedge-shaped scattered gravel deposit of unit D was likely created from a filled fault-controlled depression (Fig. 12). However, like the 1999 cracks, which were invisible in this trench, fractures that form this fissure filled by gravelly unit D and were almost invisible because of the unstratified nature of unit C. In fact, the fractures related to post-events were not expected to be visible in unit C. Even the fractures those related to the 1999 earthquake were not visible. There could have been some fractures in unit C surrounding the fill-unit (unit D), though these were not sufficiently evident. As is common in strike-slip faulting, the fissure filling is wedge-shaped. No downward continuation of the fault zone is visible within the lowest massive clay deposit (unit C) below unit D. The fissure-fill package was probably deposited against the free faces of fault scarps that were formed in unit C during this event (**event D)**. Thus, the post-depositional unit (unit D) that filled this local depression, post-date **event D**. A sample (R 28325/3) from the bottom tip of the fill (Fig. 12), that represents the closest post-date for the event, yielded an accelerator mass spectrometry (AMS) calibrated radiocarbon age of AD 890–1000 (Table 1). Thus, the dates of AD 890 and AD 1000 antedates the upper part of the fill and post-dates **event D**, respectively.

3.5. Kaledibi-1

The Kaledibi-1 trench was excavated across the surface break of the 1999 rupture in late-summer at the Kaledibi site (Fig. 8). The geomorphology shows a clear south-facing scarp in the trench site and the 1999 surface rupture consisted of approximately 15 cm southside-down vertical and 350 cm of right-lateral offset along this scarp. The western wall of the exposure was mapped at the scale of 1:20 in a short time period due to collapse risk of the unstable walls that is common due to the shallow groundwater-table along the Düzce fault. The excavation revealed three clear faults (a, b and c), each of which cut through south-dipping (10° to 20°) alluvium. Strike-slip offsets along the faults especially appear to be juxtaposed laterally with dissimilar stratigraphic sequences across them. Therefore, trench stratigraphy consists of four structural blocks that are fault-bounded (Fig. 13). All blocks are blanketed by silty clay of the uppermost part (~ 125 cm) of unit A that contain some brick pieces, are traced continuously across the trench.

Fault “c” extends all the way to the current ground surface where it meets the horizon of the 1999 earthquake. The northernmost structural block (north of fault c) is characterized by a 40-cm-thick weakly consolidated sand of unit B and fine sand of unit D below. They were overlain by the unstratified silty clay bed deposits of unit A. On the other hand, the interfingering sand (unit C) and silty clay (unit A) deposits overlay at least a 1.5-m-thick gently south-dipping poorly sorted sandy gravel deposit of unit E in the neighbor block between fault “c” and fault “b”. The deeper extension of unit E remains below the trench bottom. The other structural block between the third and fifth meters, between faults “a” and “b”, is characterized by poorly sorted unstratified sandy gravel of 40-cm-thick unit F. This unit grades downwards into well-sorted unstratified gravel of unit G, which are blanketed by the silty clay bed of unit A and interfingering sandy silt of unit C above as described above in the neighbor block. Faults “a” and “b” likely terminated in unit A, and the un-faulted unit C overlie the upper terminations of these faults. Both faults have narrow and well-defined zones. Fault “a” is characterized by its steep slope to the south and juxtaposes units F and G and lower part of unit A. Due to its slope, it may have had a significant vertical component compatible to the geomorphology and scarp formed by the 1999 event. On the other hand, fault “b” is vertical. Conspicuous faulting of unit E, against units F and G, juxtaposes dissimilar stratigraphic sequences, suggesting that it probably experienced significant strike-slip motion. Deep angle of the strata to the north of the fault is larger (25° to the south) than the layers to the south, possibly indicating that the fault may have a south-side-down vertical component. The fault plane terminates at the horizon of an event within 40 cm of the bottom part of unit A below the interfingering between the sand of unit C. The faulting event related to fault “b” was referred to as **event B**. The exact location of the event horizon within 40 cm of the bottom part of the unit A could not be determined because faults were could not be followed in unstratified deposits of unit A. A successfully dated peat sample (R28325/5) collected in the lowest part of unit A and just above unit F (Fig. 13) yielded AMS-calibrated radiocarbon age ranges of 400 – 230 BC, with the most probable date ranges being 290 – 230 BC (Table 1). This sample pre-dates **event B** and unit C.

4. Timing The Earthquakes

In this study, the excavations exposed evidence for seven earthquakes since about 1740 BC along the Düzce fault, including the 1999 surface break. Due to the unfavorable stratigraphy along the Düzce fault, we were mostly able to detect only one paleo-earthquake in each trench with each earthquake detected in different trenches. High water content and high risk of collapse made deepening the trenches quite difficult, if not impossible, to find events in series along the Düzce fault that bounds the southern border of the wetland part of the Düzce basin. Due to time constraints related to trench excavation difficulties, the trenches only reveal 2-D cross-sections of the geologic records perpendicular to the fault, and thus provide information about timing but not offset. The age samples were carefully collected right next to the event horizons. Using seven radiocarbon (14C) age determinations of the samples that pre-date or post-date events, a sequential model is suggested in this study. Pre-dated **event A** (1740 BC) and **event C** (AD 440) in Töngelli-1 and Bend-1 trenches, respectively; post-dated **event D** (AD 1000) and **event E** (AD 1290) in Bend-3 and Töngelli-3 trenches, respectively and pre- and post-dated **event F** (AD 1400 and 1800) in Töngelli 1 trench were exposed along the Mengencik segment. Furthermore, pre-dated **event B** (400 BC) in Kaledibi-1 trench was exposed along the Aydınpınar segment (Table 1). **Event G** (November 12, 1999 rupture) was clearly observed in all trenches.

A linear least square analysis of the maximum limit values of calibrated probability curves of post-dates for **events F, E** and **D** (Table 1) in a sequential serial (Fig. 14) gave a good root mean square (RMS) score. The scores are 0.95 and 0.98 based on 95.4 % and 68.2 % probability curve areas, respectively for the serial that does not include the 1999 event. The scores are the same for the serial when the 1999 event was set as the intercept for the trend line. In this serial, events F, E and D represent penultimate, pre-penultimate and third earthquakes, respectively, and are termed first, second and third events, respectively in this study. Emre et al. (2002, 2004) suggested AD 1750 while Pantosti et al. (2008) suggest AD 1900 for the post-date of the penultimate event (1st event, **event F**). Using these dates instead of our post-date value of 1800 (AD), the maximum limit did not change the RMS, according to the 68.2 % probability curve. However, both suggested dates overestimated our maximum values (1600 and 1670) for the highest top two probability areas of the 68.2 % probability curve for **event F** (sample R26946/5) (Table 1). For this reason, our suggested post-date appears more appropriate, and was used for the serial. Another post-date, AD 1640 (sample KW-02) that was also suggested by Pantosti et al. (2008) for the penultimate event, also overestimated the maximum limit (1600) from the highest (33.2 %) probability area of the probability curve (Table 1). All three dates suggested by these other studies (AD 1640, 1750, 1900) greatly overestimate our suggested maximum limit date of post-dating sample R28325/10 for **event E** (2nd event). Indeed, setting any one as a post-date for event E markedly increases the error in our linear least square fit model. Emre et al. (2002, 2004) and Pantosti et al. (2008) also suggested post-dates of AD 1050 and 1020. Using these dates instead of the maximum values of 1000 or 1030 (AD) from our post-date curves according to 68.2 % or 95.4 % probability, respectively, did not change the RMS. However, they both overestimates our maximum value (1000) from the 68.2 % probability curve of the post-date (sample R28325/3) for **event D**. In addition, setting any date to post-date event C that pre-dated by our sample R28325/9 increases the error value of the post-dating model fit. Consequently, according to the post-dating linear fit line (Fig. 14) of the sequential serial set, the upper bound for the range of the

recurrence interval zone between pre- and post-dates, is about 400 years. The post-dating fit line is based on the maximum values of 68.2 % probability ranges of post-dates introduced in our study.

After completing the linear least square analysis, we defined another linear serial to determine and test a pre-dating linear fit model based on pre-dating samples of events (Fig. 14). Previously suggested dates of AD 1650 (Emre et al., 2002; 2004) and 1685 (Pantosti et al., 2008), for pre-dating the penultimate rupture (1st event, **event F**), exceeds maximum limits of 33.2 % and 61.7 % (33.2 % plus 28.5 %) areas of probability curves, respectively, for the post-date of event F (sample R26946/5) suggested in the current study. Another pre-date of AD 1280 (sample CIN1-W500) suggested by Pantosti et al. (2008) underestimates the minimum value from the 68.2 % probability curve of pre-dating sample R26946/4 for **event F**. Thus, using the pre-date from Pantosti et al. (2008), instead of the pre-date determined from our sample, is not adaptable for **event F**. On the other hand, the sample CIN1-W500 may pre-date **event E** that post-dated by the maximum value of 68.2 % probability curve of sample R28325/10 (Table 1). In addition, there are two pre-dates of AD 685 and AD 665 from Pantosti et al. (2008) and Emre et al. (2002, 2004) respectively. These dates underestimate the AD 1280 pre-date (Pantosti et al., 2008) suggested for **event E** in this study. However, both could pre-date **event D** that was post-dated by sample R28325/3 determined in the current study. According to this timing, pre-dates of **events F, E and D** appear to be in a linear sequence, as are their post-dates. As a result, using pre-dating samples from previous studies for **event E** and **D**, results in a linear sequential serial for the last five ruptures in the following order: **event G** (1999 rupture), **F, E, D** and **C**. On the other hand, two older pre-dated events (**events A** and **B**) seem to indicate irregularity in this sequence. Unrecognized earthquakes may eliminate the irregularity between **events C** and **A**. A linear least square analysis of the pre-dates of **events F, C, B** and **A** that were set as penultimate, forth, sixth and ninth rupture, respectively (Fig. 14) gave the best RMS error value for our data (0.99). The RMS was the same for both calculations based on lower limits of 95.4 % and 68.2 % probability areas of the calibrated curves. AD 1280 and AD 685 pre-dates (Fig. 14) from Pantosti et al. (2008) are adaptable to our serial for **event E** and **D**, respectively. AD 665 pre-date also is appropriate for **event D** but AD 685 fits better to the sequence. The error from fitting the model did not increase when using these samples from Pantosti et al. (2008). Therefore, they confirm the suggested recurrence interval based on linear sequential serial fit from pre-dating samples in the current study. In addition, the pre-dates of AD 1650 and 1685 suggested by Emre et al. (2002, 2004) and Pantosti et al. (2008), respectively, corroborate the position of **event F** in the time scale found in the current study. According to the pre-dating fitted linear line (Fig. 14) based on this sequential serial set using the data determined in the current study, the lower bound of the range of the recurrence interval zone is about 394 years based on 68.2 % probability curves of the samples used.

In summary, according to the linear sequential event serial (SES) in this study, **events G**, **F**, **E**, **D** and **C** in order represent the 1999 Düzce, penultimate, pre-penultimate and third earthquakes, respectively and the oldest **events B** and **A** represents sixth and nineth earthquakes, respectively (Fig. 14). The sequence of dates determined in our study and previously determined dates of these paleoseismic events, suggest periodicity for large earthquakes along the Düzce fault. According to the pre- and post-dating linear sequential least square fits based both on 68.2 % and 95.4 % probability curve limits of the samples in

the SES model, the earthquake recurrence interval ranges between 394 and 400 years and between 384 and 460 in a very narrow zone, respectively (Fig. 14). The date of the 1999 Düzce rupture remains in the recurrence interval zone (envelope) between the linear fits (Fig. 14). In other words, the 1999 earthquake has been predicted quite accurately, although based on limited data available. In addition, the range of the zone (384–460 years) is narrow, ± 38 years, based on 95.4 % probability curve limits.

Instead of using maximum and minimum edges of probability curves for pre- and -post-dates of events, whole probability distributions of the dates were used to estimate probability distribution of any target event in the SES (Fig. 14). In this operation, called probability distribution-based method (PDBM), based on Monte Carlo sampling, random sampling was made from probability distributions of the pre- and post-dates of samples in the SES model (Fig. 14). One sample was used for each of the probability distributions to generate a serial based on SES. Linear least square regression was applied to the 100000 random serials generated from randomly sampled values from the probability distributions of dates introduced in this study. Thus, a sufficient number of series were produced for all possible combinations of the sampled points from the probability distributions in SES. More sampling was done for higher probability regions of the distributions. A probability value for the linear fit model that was produced for each of the 100000 randomly sampled serials depended on the sum of values of sampled probability levels on probability distributions for each dating sample. Probability distribution for a targeted event position in the SES was calculated based on the probability values for the linear fits. In this process, **event G** (Fig. 14), the date of which is known (November 12, 1999 Düzce earthquake), was first taken as the target in calculations to test both the SES model and the PDBM. Calculated probability distribution for this target (**event G**) ranges between 1933–2005 with a 68 % probability (± 36 years error). This test suggests that when the SES model is used, it allows us to predict the November 12, 1999 earthquake quite accurately (Fig. 15). After that, the next event (first future earthquake, **event H**) was targeted. The probability distribution of this target event was calculated using the PDBM that was tested with the 1999 earthquake and the SES model (Fig. 15b). According to this estimation there is a 68 % probability that the next earthquake rupture will occur between 2328–2392 along the Düzce fault with a recurrence interval of about 391 ± 34 years. Based on the November 12, 1999 earthquake, using this recurrence interval the predicted earthquakes in any event order using the SES model are within the envelope between the sequential linear fits in Fig. 14.

5. Conclusion

Probable segmentation of the Düzce fault was configured by considering the three left stepovers along the 1999 rupture (Fig. 3). However, the sequential event serial (SES) model proposed in this paleoseismological study and uniform slip distribution of the 1999 event, suggest that there may only be a single segment. Evidence for six large earthquakes in 3750 years before the 1999 earthquake was obtained from five excavations across the middle part of the Düzce fault at three sites along two segments. Seven 14C accelerator mass spectrometry (AMS) dates for the six events were used to determine the recurrence intervals for large earthquakes. The pre- and post-dating samples for events were carefully collected right next to the event horizons. This paleoseismological trenching provides only

a preliminary information about the seismogenic behavior of the Düzce fault. The offset could not be fully assessed since the trenches revealed a 2-D cross-section of the geologic record perpendicular to the fault. In addition, unfavorable trench material in the stratigraphy and scarcity of datable material made the identification and characterization of individual paleo-earthquakes quite difficult and sometimes impossible along the fault. One of the constraining dates, either the pre- or post-date, could not be identified for most of the events. Furthermore, the lengths of ruptures of these paleo-earthquakes are not known and the event information came from different trenches. These problems provide challenges when constructing the sequential model. Nevertheless, the data suggest that the model is consistent. The model (SES) introduced in this study was described considering the maximum values of the post-dating sample date ranges and minimum values of the pre-dating sample date ranges of paleoseismic events. The upper and lower bound of the range for recurrence interval is about 400 and 394 years, respectively according to the fit lines of the sequential serial set based on dates of post- and pre-dating samples with a 68.2 % probability. Similarly, a recurrence interval of about 391 ± 34 years with a 68 % probability was also calculated based not on the limits but on whole probability distributions of the dates of samples (PDBM). Either way, the 1999 earthquake was predicted quite accurately based on the SES model suggested in this study (Figs. 14, 15). The date of this last Düzce earthquake occurred within the predicted 72-year range (1933–2005) with a 68 % probability, confirming the accuracy of our model.

6. Discussion

The written history for the region surrounding Marmara extends more than two millennia ago because İstanbul was a center of trade. Several earthquake catalogues were compiled and published for the Marmara region. Ambraseys and Finkel (1995) and Ambraseys (2002) provided a recent review of these records. In addition, Bakır (2002) reviewed historical earthquakes in Eastern Roman Constantinople (İstanbul) for the period of AD 342–1454. In contrast, the written history for the Bolu and Düzce region, which is about 500 km away from İstanbul, is not that extensive. According to Ambraseys and Finkel (1995), available data is limited to the large destructive earthquakes of the Bolu and Düzce region of prior to the September 10, **1509** earthquake. Only one episode of rupturing was identified in our excavations which occurred during, or after AD 1509, **event F**. The suggested age of **event F** is between AD 1400 and 1600 according to the highest probability regions of the probability distributions for pre-and post-dating samples (Table 1). According to Konukçu (1984), the next destructive earthquake after the **1509** earthquake was the earthquake of May 25, **1719** in the Düzce area (See also Ambraseys and Finkel, 1995). However, the date of this historical earthquake is after the maximum limit (AD 1600) of the highest probability region (32.2 %) of the 68.2 % probability distribution of sample R26946/5 which post-dates **event F**. The earthquake could only be a candidate for **event F** according to the maximum limit (AD 1800) of the 68.2 % probability distribution region of this sample with lowest probability (6.5 %). Pantosti et al. (2008) suggested linking the 19 April **1878** historical earthquake with the events from their trenches, but this earthquake was considered a local earthquake near Sapanca lake (e.g., King et al., 2001). In addition, it exceeds most of the lowest probability region of the post-dating sample with 95.4 % probability distribution. (Table 1). There is no other historical large earthquake documented in the eighteenth and the

nineteenth century in the vicinity of the Düzce area. Thus, the episode of rupture may plausibly be associated with either the **1509** or **1719** earthquakes. On the other hand, the date range that is suggested by the PDBM for **event F** was between AD 1575 and 1643 (AD 1609 ± 34) with a 68 % probability. Further, both fall outside the maximum limit of 95 % probability region of PDBM. Thus, they are not likely related to the Düzce fault.

The oldest recorded historical earthquake that has relation with the Düzce area is the **AD 967** earthquake in the Eastern Roman period (Bakır 2002) and was recorded in Bolu. An episode of rupturing was identified in the Bend-3 trench (**event D**) just before AD 1000 (Table 1), suggesting that the **967** earthquake may be what was identified as **event D**. This event was post-dated with a maximum limit of AD 1000 (sample R28325/3) and pre-dated by a sample (AD 685) from Pantosti et al. (2008). At the time of the **AD 967** earthquake, there was only a small town in the Düzce region; however, Bolu was a major city (Nevra Necipoğlu, pers. comm. 2004 and see also Konukçu 1984). For this reason, damage was likely to be better documented in the Bolu area than the Düzce region. As the **AD 1509** and **1719** earthquakes, this earthquake is out of the limits of the estimated date range for **even D** based on the PDBM. Ambraseys and Jackson (1998) associated this historical event with the Bolu fault according to Quaternary or recent fault rupture. Thus, it is likely related to the Bolu fault.

Hitchcock et al. (2003) described and reported dates for at least four and possibly five events (including 1999) that occurred in the past 2100 years along the Kaynaşlı segment. Contrary to the earthquake recurrence interval of 391 years suggested in the current study, based on PDBM, the suggestion of about 525- or 700-years recurrence interval by Hitchcock et al. (2003) underestimates one or two events. Conversely, an interval of 330–430 years suggested by Pantosti et al. (2008) is in concordance with our results. However, the penultimate earthquake that Pantosti et al. (2008) correlates with the **1878** historical earthquake, which was only 121 years before the 1999 earthquake, is inconsistent with their suggestion. On the other hand, the pre-penultimate event they proposed (AD 1495–1700) could have been a good candidate for the penultimate event that is suggested in the current study. However, the AD 1650–1750 range suggested by Emre et al. (2002, 2004) for this event is not consistent with the recurrence interval estimates presented in the current study. Assuming an average slip of 350 cm (average slip of the 1999 earthquake) for the Düzce fault, the calculated slip rate is 8.7–11.2 mm/a based on the recurrence interval presented here (391 years). This rate is consistent with paleoseismological study of Pantosti et al. (2008) that calculated a slip rate of 6.9–15.6 mm/a.

Declarations

Acknowledgement

This study was mostly supported by a project with 01T201D ID from Boğaziçi University Research Fund and was partially funded by Boğaziçi University Kandilli Observatory and Earthquake Research Institute. I am grateful to Esen Arpat for suggesting critical problems, inspiring guidance from initial field work to the completion of the study and critically reviewing the manuscript. I thank Hadi Özbal, Caroline Finkel and

Mehmet Özdoğan for inspiring guidance concerning historical earthquakes. I am grateful to Nevra Necipoğlu, Aslı Özyar and Mevlüde Bakır for valuable information about historical earthquakes.

Conflict of Interest: The authors declare that they have no conflict of interest.

References

Ambraseys NN, Finkel CF (1995) The Seismicity of Turkey and Adjacent Areas: A Historical Review. 1500-1800. Eren Yayıncılık ve Kitapçılık Ltd. Şti., İstanbul. ISBN: 975-7622-38-9

Ambraseys NN, Jackson JA (1998) Faulting associated with historical and recent earthquakes in the Eastern Mediterranean region. Geophys J Int 133:390-406. https://doi.org/10.1046/j.1365-246X.1998.00508.x

Ambraseys NN, Zatopek A (1969) The Mudurnu Valley, West Anatolia, Turkey, Earthquake of 22 July 1967. Bull of Seismol Soc of Am 59:521-589.

Arpat E, Herece E, Komut T, Şentürk K (2001) 1999 Kocaeli ve Düzce Depremlerine neden olan fayların Marmara Bölgesinin sismotektonik yapısı içindeki yeri. 54th Geological Congress of Turkey, May 7-10, 2001, Ankara, Proceeding no: 54-29.

Bakır M (2002) Impact and Consequences of Earthquakes in Byzantine Constantinople and its Vicinity, A.D.342-1454. Dissertation, Boğaziçi University

Bronk Ramsey C (1995) Radiocarbon Calibration and Analysis of Stratigraphy: The OxCal Program. Radiocarb 37:425-430. https://doi.org/10.1017/S0033822200030903

Bronk Ramsey C (2001) Development of the Radiocarbon Program. OxCal Radiocarb 43:355-363. https://doi.org/10.1017/S0033822200038212

Bronk Ramsey C (2004) Online version of the OxCal program, Ver. 3.9. Oxford Radiocarbon Accelerator Unit, http://www.rlaha.ox.ac.uk/orau/index.html. Accessed 11 August 2004.

Emre Ö, Duman TY, Toda S, Okuno M, Dogan A, Özalp S, Tsutsumi H, Tokay F, Haraguchi T, Kondo H, Sugito N, Nakamura T (2002) Paleoseismicity of Düzce Fault in the Last Millennium, North Anatolian Fault Zone (NAFZ), Turkey. 1st International Symposium of the Faculty of Mines (İTÜ) on Earth Sciences and Engineering 16-18 May 2002, İstanbul, Turkey, 59.

Emre O, Toda S, Doğan A, Awata Y, Tokay F, Ozalp S (2004) Paleoseismic Behaviour of the Karadere Fault Between İzmit and Düzce Ruptures in 1999, North Anatolian Fault, Turkey. 32nd IGC, Florence 2004 - Abstracts.

Hitchcock C, Altunel E, Barka A, Bachhuber J, Lettis W, Kozacı Ö, Helms J, Lindvall S (2003) Timing of Late Holocene Earthquakes on the Eastern Düzce Fault and Implications for Slip Transfer between the

Southern and Northern Strands of the North Anatolian Fault System, Bolu, Turkey. Turk J of Earth Sci 12:119-136.

Ketin İ (1969) Kuzey Anadolu Fayı Hakkında. MTA Bull 72:1-27.

King GCP, Hubert-Ferrari A, Nalbant SS, Meyer B, Armijo R, Bowman D (2001) Coulomb interactions and the 17 August 1999 Izmit, Turkey earthquake. C R Acad Sci IIA 333(9):557– 569. https://doi.org/10.1016/S1251-8050(01)01676-7

Komut T (2005) Paleoseismological Studies on Düzce Fault and Geological Data on the Seismogenic Sources in the Vicinity of the Düzce Area. Dissertation, Boğaziçi University

Konukçu E (1984) Düzce Tarihi (İlk Devirlerden Cumhuriyete). Türkiye İmar Turizm ve Sanayi Mecmuası 18:12-23.

Öcal N (1959) 26 Mayıs 1957 Abant Zelzelesi. Maarif Vekaleti, İstanbul Kandilli Rasathanesi, Sismoloji Yayınları, 4, İstanbul

Pantosti D, Pucci S, Palyvos N, De Martini PM, D'Addezio G, Collins PEF, Zabci C (2008) Paleoearthquakes of the Duzce fault (North Anatolian Fault Zone): Insights for large surface faulting earthquake recurrence. Journal of Geophysical Research 113, B1. Doi: 10.1029/2006JB004679

Stuvier M, Reimer PJ, Bard E, Beck JW, Burr GS, Hughen KA, Kromer B, McCormac FG, van der Plicht J, Spurk M (1998) INTCAL98 Radiocarbon age calibration, 24,000-0 cal BP. Radiocarbon 40:1041-1083. https://doi.org/10.1017/S0033822200019123

Şaroğlu F, Emre Ö, Kuşçu İ (1992) Active Fault Map of Turkey. General Directorate of Mineral Research and exploration (M.T.A), Ankara

Taşman CE (1944) Gerede - Bolu depremi. MTA Bull 1:1-31.

Table 1

Event	Laboratory Sample Number	^{14}C age (Conventional, B.P.)	Calibrated Date in Terms of Confidence Intervals					
			interval of 95.4% probability			interval of 68.2% probability		
			min.	max.	% of area	min.	max.	% of area
G								
F	R26946/5 *	266±50	1480	1680	78.5	1520	1600	33.2
			1730	1810	14.3	1620	1670	28.5
			1930	**1950**	2.5	1780	**1800**	6.5
	R26946/4	488±50	**1310**	1360	9.8	**1400**	1460	68.2
			1380	1500	85.6			
E	R28325/10 *	757±40	1190	**1300**	95.4	1230	**1290**	68.2
D	R28325/3 *	1085±40	880	**1030**	96	890	930	22.9
						940	**1000**	45.3
C	R28325/9	1571±40	**410**	600	65.4	**440**	540	68.2
B	R28325/5	2272±40	**400 BC**	340 BC	38.7	**400 BC**	350 BC	33.7
			320 BC	200 BC	56.7	290 BC	230 BC	34.5
A	R26946/1	3367±45	**1750 BC**	1520 BC	95.4	**1740 BC**	1710 BC	11.5
						1700 BC	1600 BC	52.9
						1550 BC	1530 BC	3.8

Table 1. Radiocarbon dates of peat samples.

Notes: Calibrations according to atmospheric data from Stuiver et al (1998) using Calib 3.9 software (Bronk Ramsey, 1995, 2001 and web). Radiometric ages were obtained at the Rafter Radiocarbon Laboratory (RAFTER), Institute of Geological and Nuclear Sciences.

* post-dating sample. Others, pre-dating samples.
Calibrated Dates in Terms of Confidence Intervals: Bold represents maximum and minimum limits of probability curves of calibrated dates for post- and pre-dating samples, respectively.

Figures

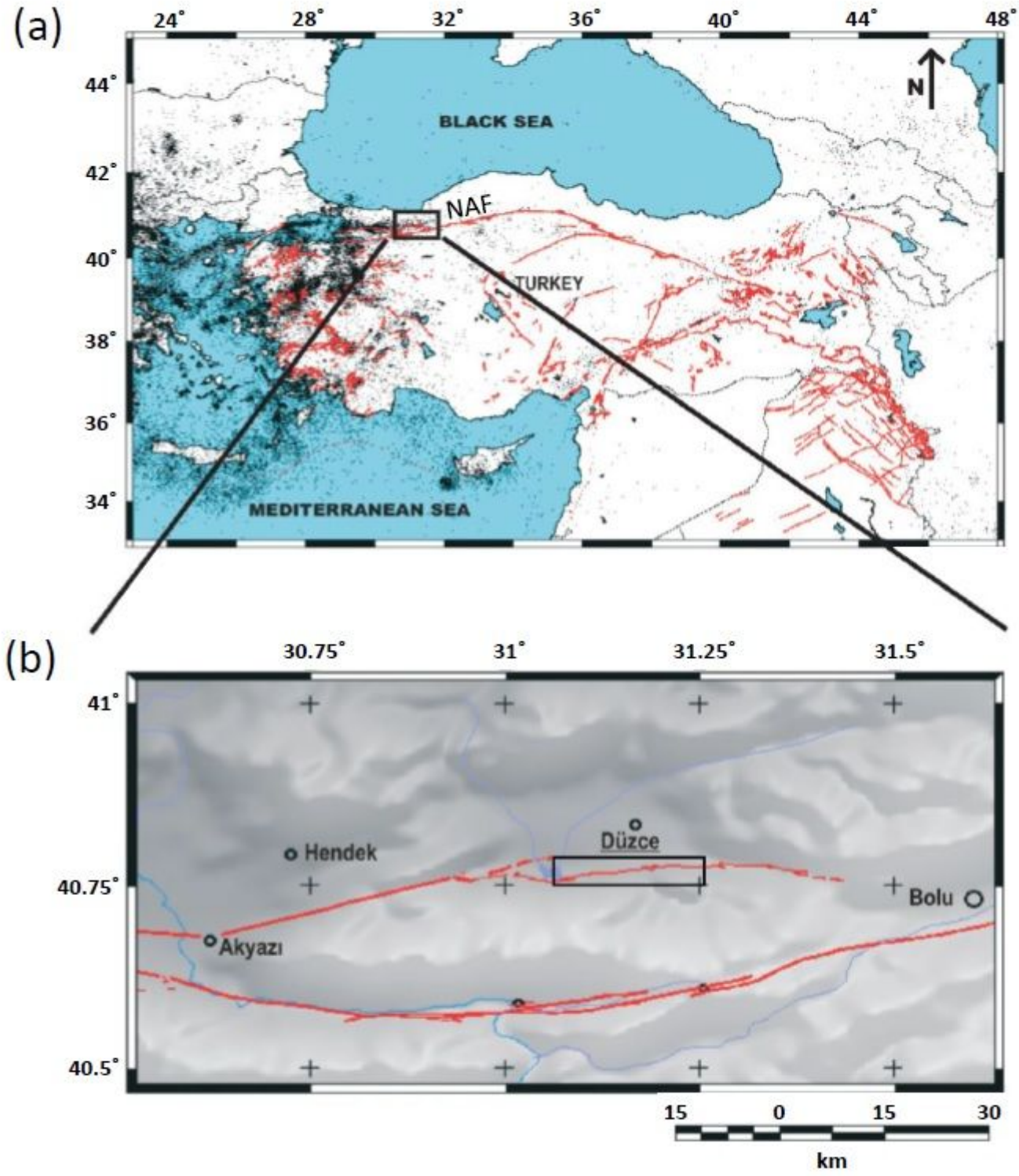

Figure 1

Location of the study area. (a) Seismicity and active fault map of Turkey and surrounding area. Black dots are earthquakes from USGS catalogue. Red lines are active faults (Şaroğlu et al. 1992); (b) The study area (rectangle) and surrounding region on southwest-shaded topographic relief. Red lines are surface breaks of earthquakes since 1944. The Düzce fault extends along the southern border of the Düzce basin.

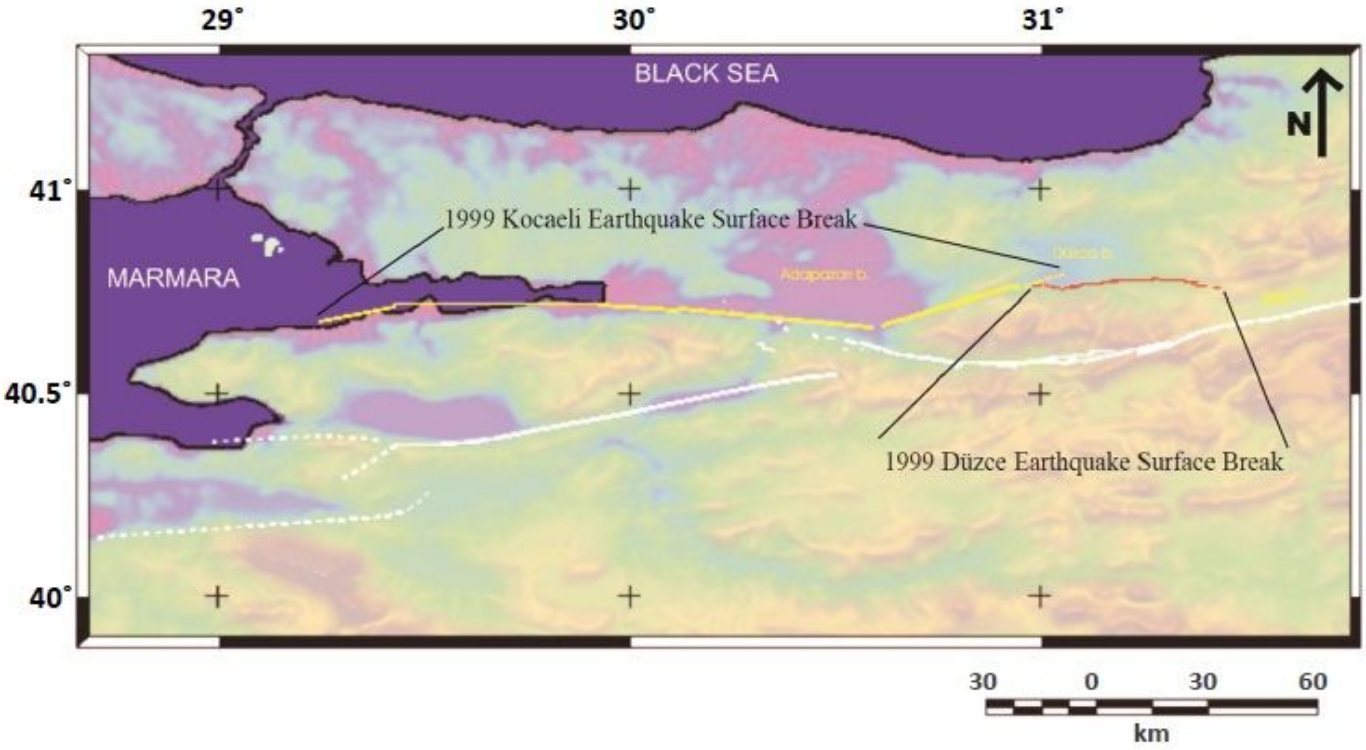

Figure 2

The 1999 ruptures and the active faults in the surrounding region. Red and yellow lines are 1999 Kocaeli and Düzce ruptures, respectively. The 1999 Düzce earthquake produced about 42-km dextral rupture.

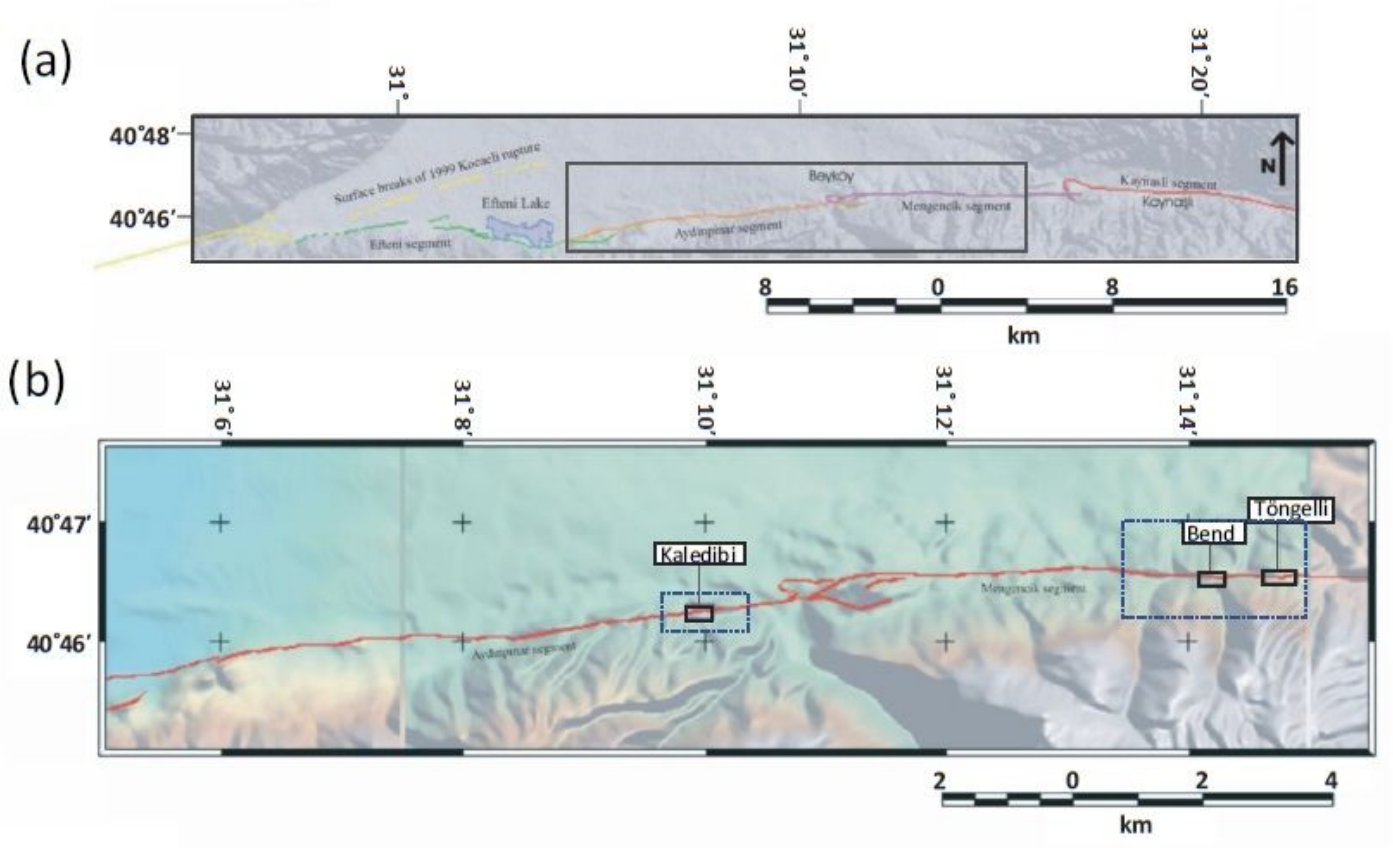

Figure 3

Probable segments of Düzce fault and paleoseismological observation sites along them. Background is southwest-shaded relief topography. (a) Locations of four probable segments along the Düzce fault. (b) Trenching site locations. The map area was shown by a rectangle in ‘a’. There are three trenching in Kaledibi, three in Bend and five in the Töngelli sites in this study. The dotted rectangels on the left and right are the map areas of figures 4 and 8, respectively.

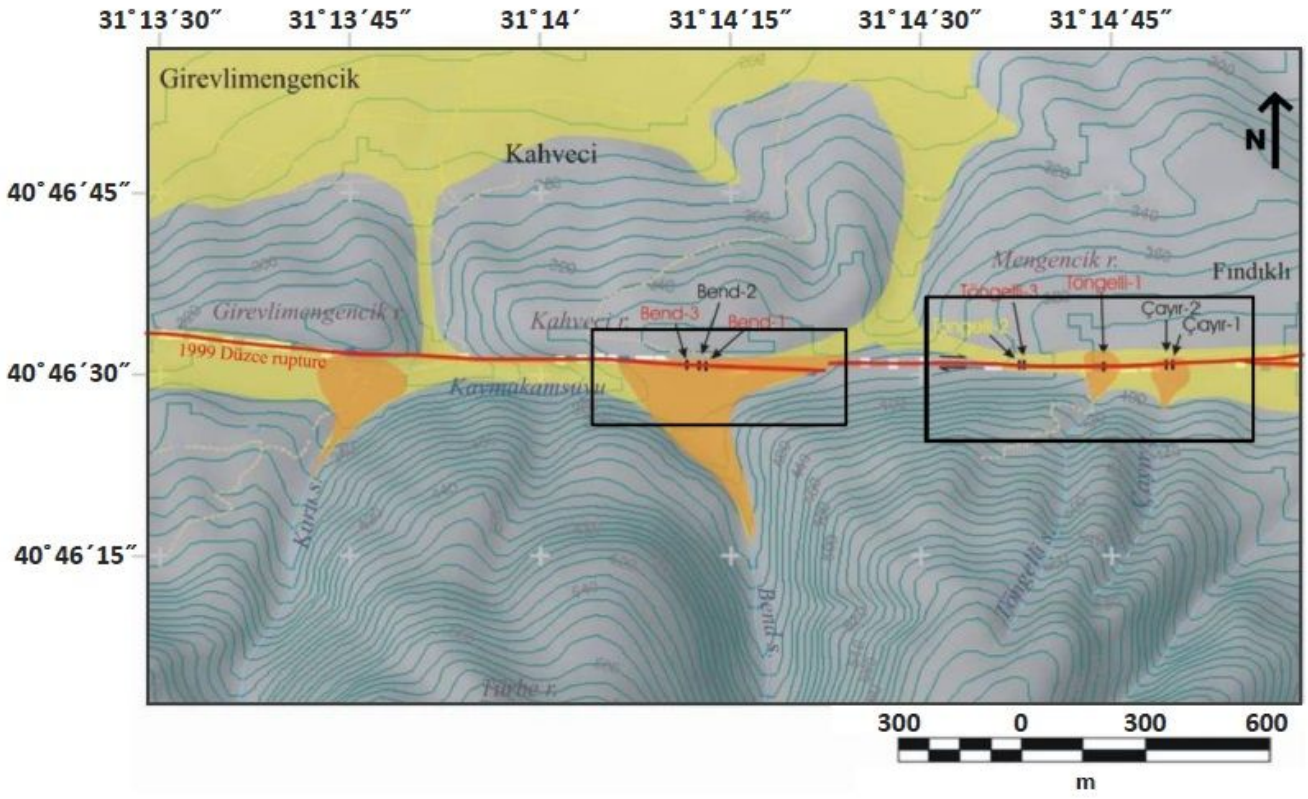

Figure 4

The Töngelli and Bend trench sites on topographic map. Contours with 10 m interval were draped on the southwest-shaded topograhic relief. The map area was shown in figure 3. The rectangles on the right and left are the Töngelli and Bend sites shown in figures 5 and 7, respectively. Girevlimengencik, Kahveci and Mengencik shutter ridges in the north of the 1999 fault rupture (red line) are lined up in front of the northern slope of the Almacık mountain. The trenches with names colored in red contain dated events. The trenches with names colored in yellow contain events. Other trenches do not have visible stratigraphy. The areas shaded with yellow and orange are Quaternary alluvium and alluvial cones of streams, respectively. The Çayır-1 and Çayır-2 trenches excavated on alluvial fan of a relatively small stream (Çayır stream) and do not have visible stratigraphy.

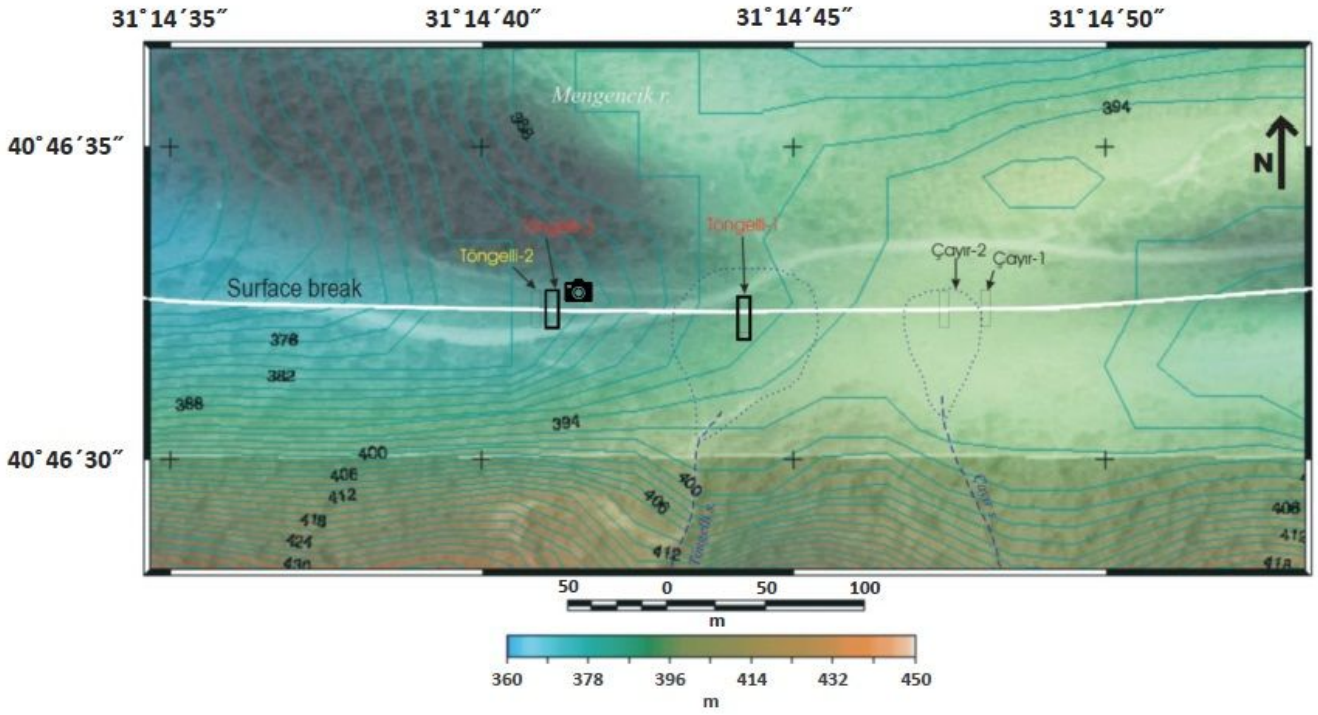

Figure 5

Töngelli and Çayır paleoseismological sites. The color scale shows elevation. Semi-transparent south-shaded topographic relief was draped on aerial photo. Topographic contour interval is 2 m. Trenches with names colored in red contain dated events. Trenches with names colored in yellow contain events. Other trenches do not have visible stratigraphy. Dotted lines represent boundaries of the alluvial fans and dashed lines are streams. See figure 4 for the location of the map area.

Figure 6

A surface deformation photo of the 1999 rupture in Töngelli site near Töngelli-3 trench. See the figure 5 for the location of this northeast-facing photo. The narrow trough structure formed by 1999 earthquake continues more than 50 m to the east.

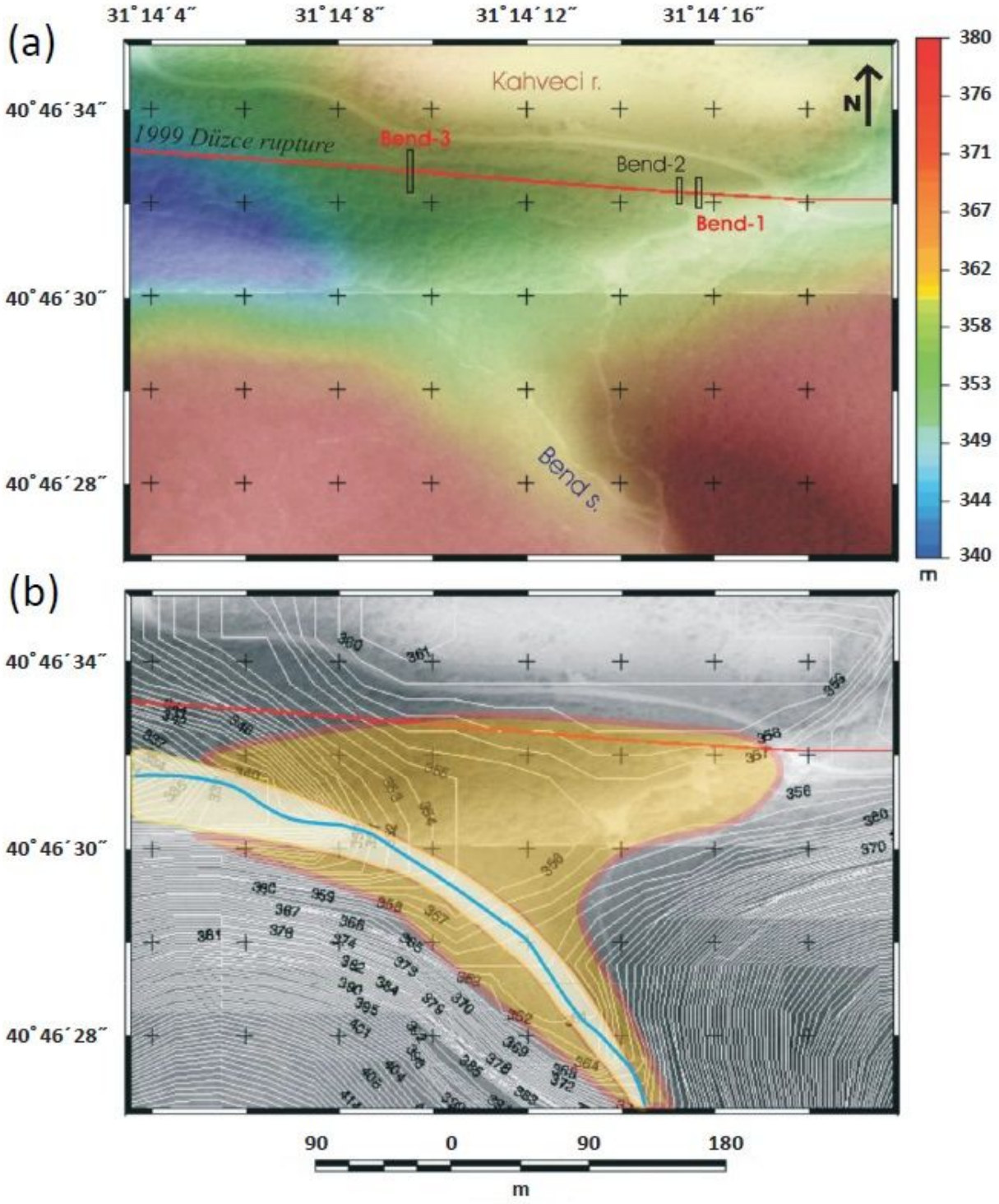

Figure 7

Bend trench site. Bend 1, 2, and 3 trenches were on the alluvial cone of the Bend stream. Maps (a) and (b) are proportional. See figure 4 for the location of the map area. (a) Semi-transparent aerial photo draped on southwest-shaded topographic relief. Color scale is elevation. Red line is 1999 surface rupture. Rectangles are trench locations. No event was recognized in trenches with black font name. Events were recognized and dated in trenches with red font name. (b) Quaternary development of Bend stream fan

shaded with yellow on southwest-shaded semi- transparent topographic relief map draped on aerial photo. Topographic contour interval is 1 m. Alluvial fan of the Bend stream was trapped by Kahveci shutter ridge. Light yellow zone shows the bed of the stream. The fan propagated back into the valley filling it towards the uphill direction because it was blocked from north by the Kahveci ridge. In addition, because of this blockage, normal fan geometry on the topography does not exist here.

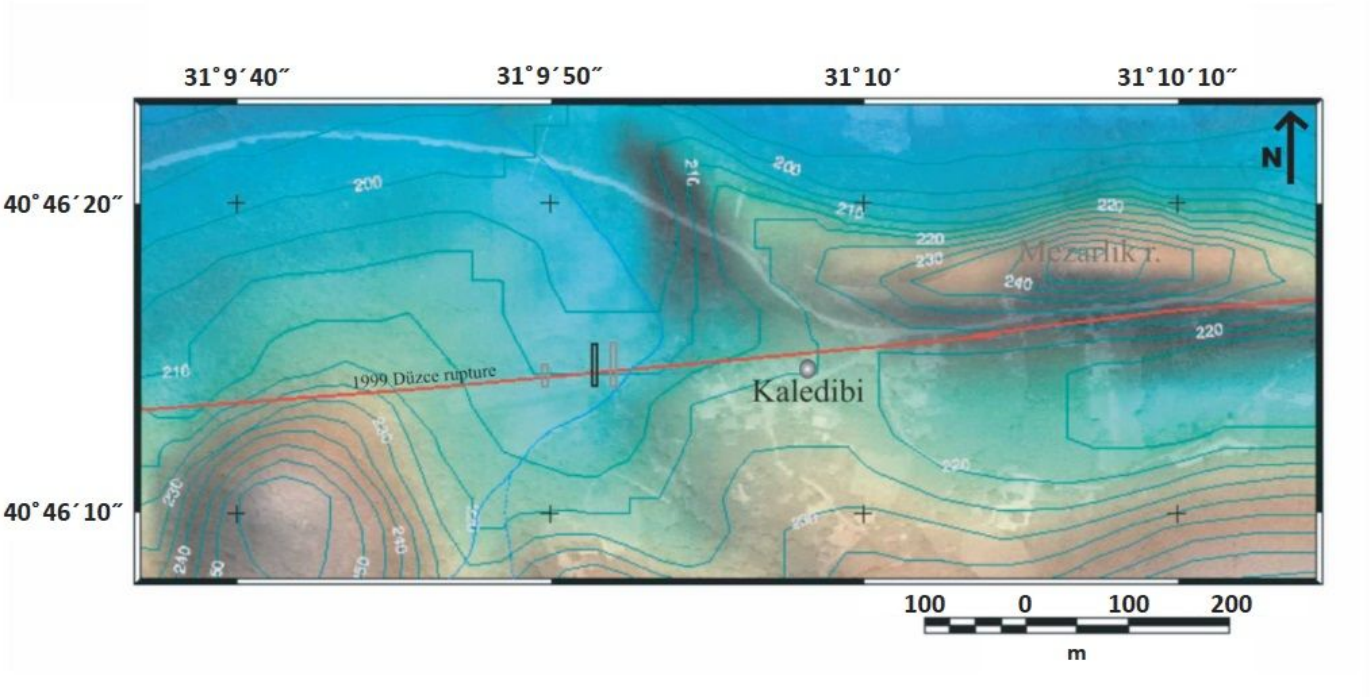

Figure 8

Kaledibi trench site. The area of the map was shown in Figure 3b. Black rectangle on the map represents the Kaledibi-1 trench. The other trenches that were shown by gray rectangles are exploratory trenches. Semi-trasnparent colored south-shaded topographic relief map was draped on aerial photo. Topographic contour interval is 5 m.

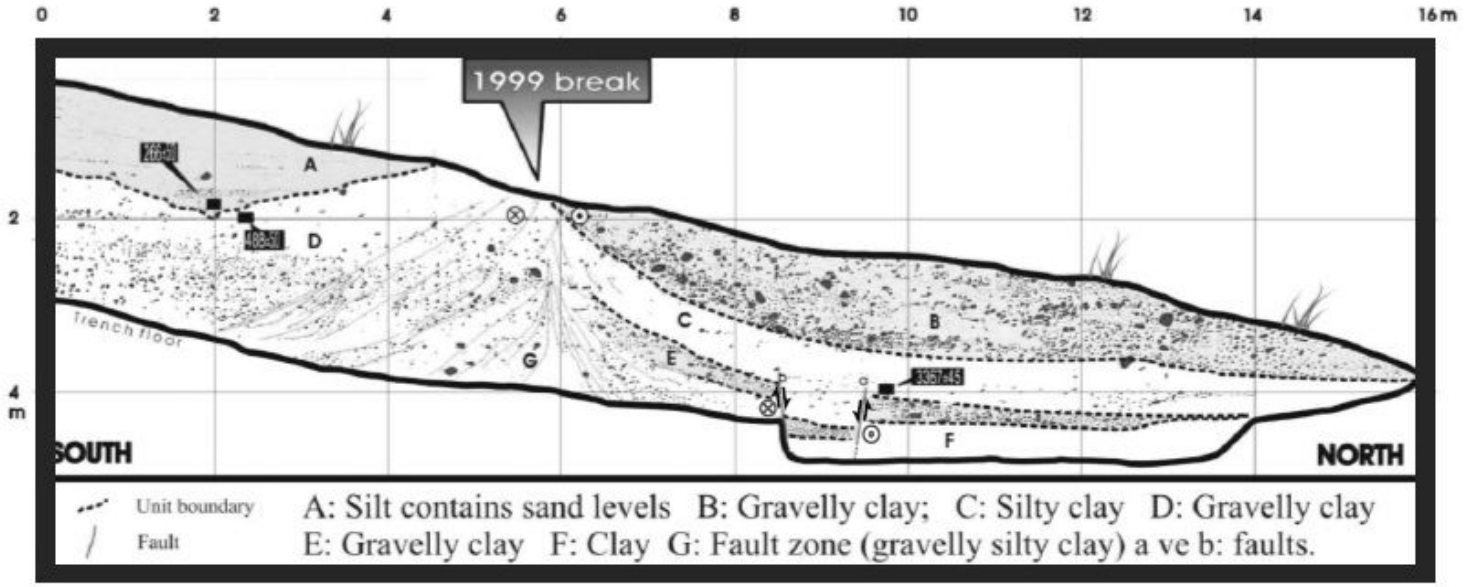

Figure 9

Log of Töngelli-1 trench. See figure 5 for the trench site location. Event A is a pair of normal faulting between 8th and 10th meters. Event F is a compressional feature between 2th and 8th meteres. There are two structural blocks that are flanks (left and right of the 5.5th meter station) of the compressional structure in the exposure. There is a local depression between 0 and 4th meters between the compressional structure and slope of the hill. Unit A is the fill-deposit in this depression. Carbon sample location is outlined in black rectangles. The conventional 14C ages for the samples are given in the rectangles (Table 1).

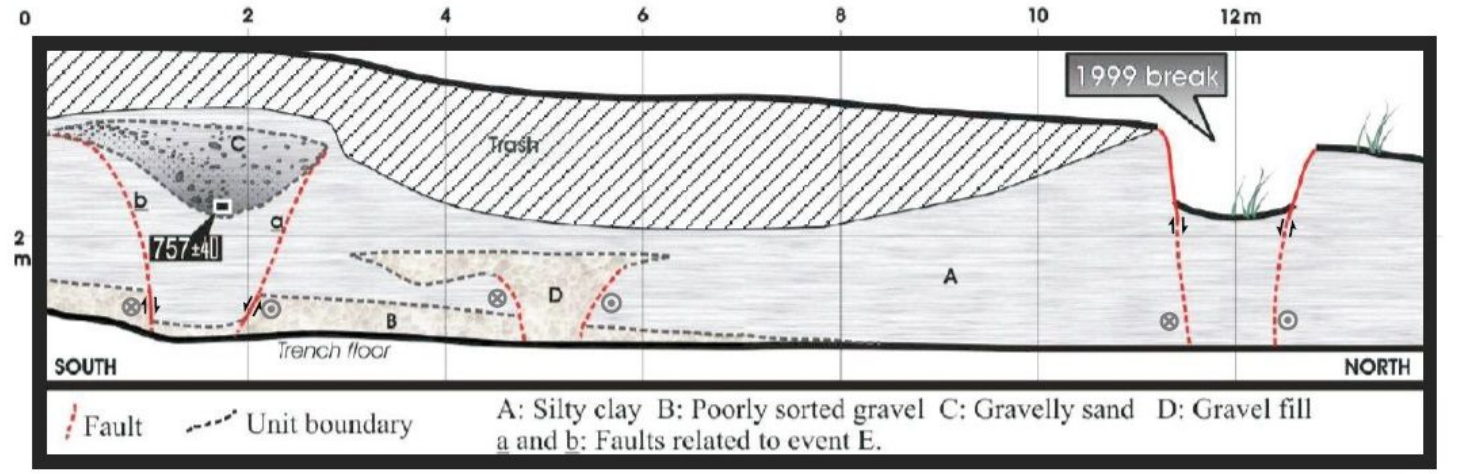

Figure 10

Log of the Töngelli-3 trench. See figure 5 for the trench site. Uniform deposition of massive silty-clay of unit A, was probably interrupted (locally) by the deformation related to event E around 2nd meter from

South. Unit C fills the fissure that formed on the event horizon about 70 cm depth. The other fissure-fill (unit D) represents another event. All the events including the 1999 rupture have similar deformation geometry in this exposure. Both the sizes and shapes of the fissures are like each other. A typical trough morphology of the 1999 rupture was clearly observed on the site (Fig. 6). Event E was dated with a carbon sample outlined in black square (R28325/10). The conventional 14C age for this sample is given in the rectangle (Table 1).

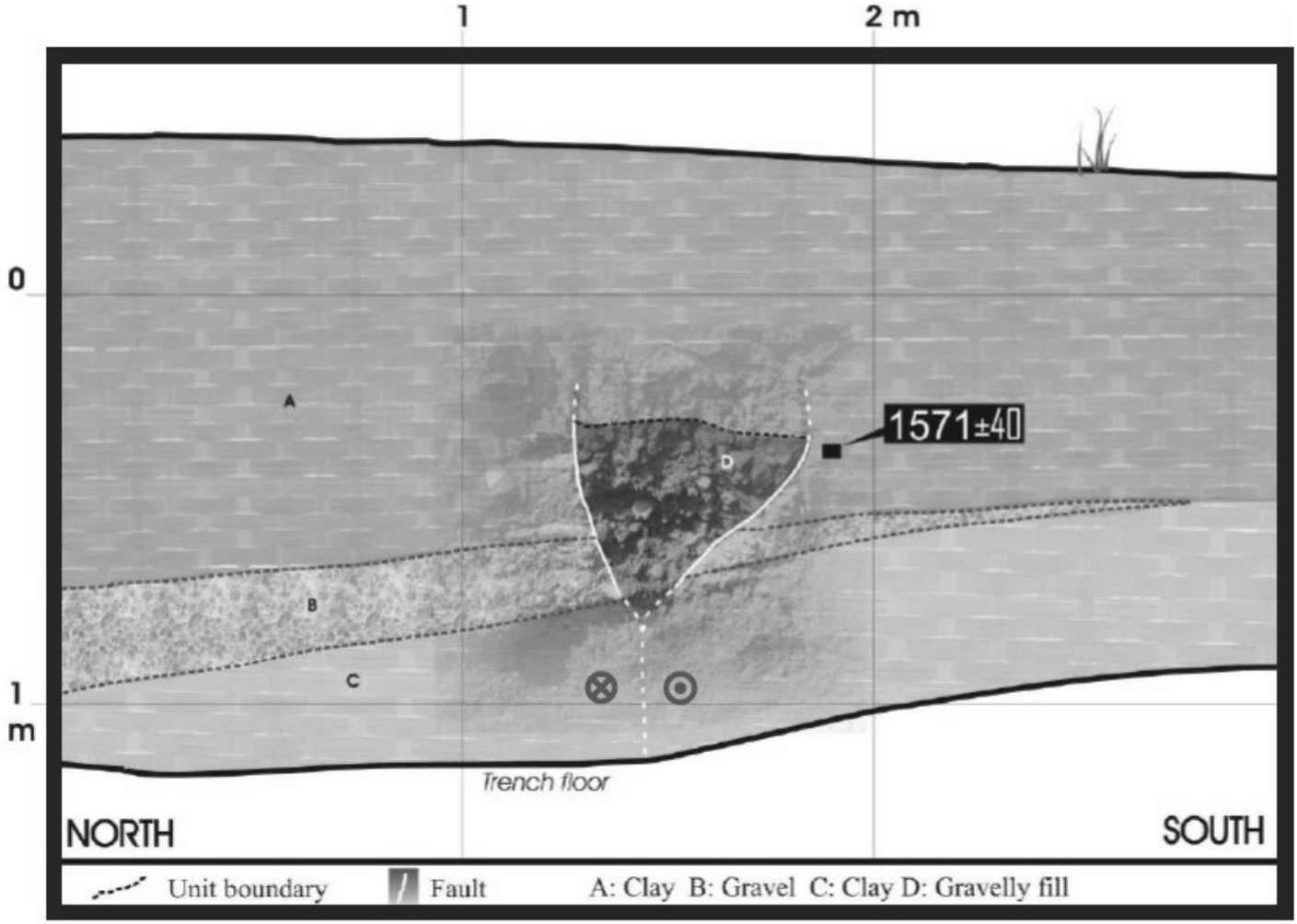

Figure 11

Bend-1 trench exposure. See figure 7 for the trench site. There is one paleo-event (event C) in Bend-1 trench. Event region was shown by a rectified picture draped on log with radial transparency. There is a clear wedge-fill (unit D) that contains gravel deposit. The surface rupture of the 1999 event that crosscut the trench is about 1 m north beyond the left boundary of the section. Carbon sample location is outlined in black square (R28325/9, Table 1). The conventional 14C age for this sample is given in the rectangle (Table 1).

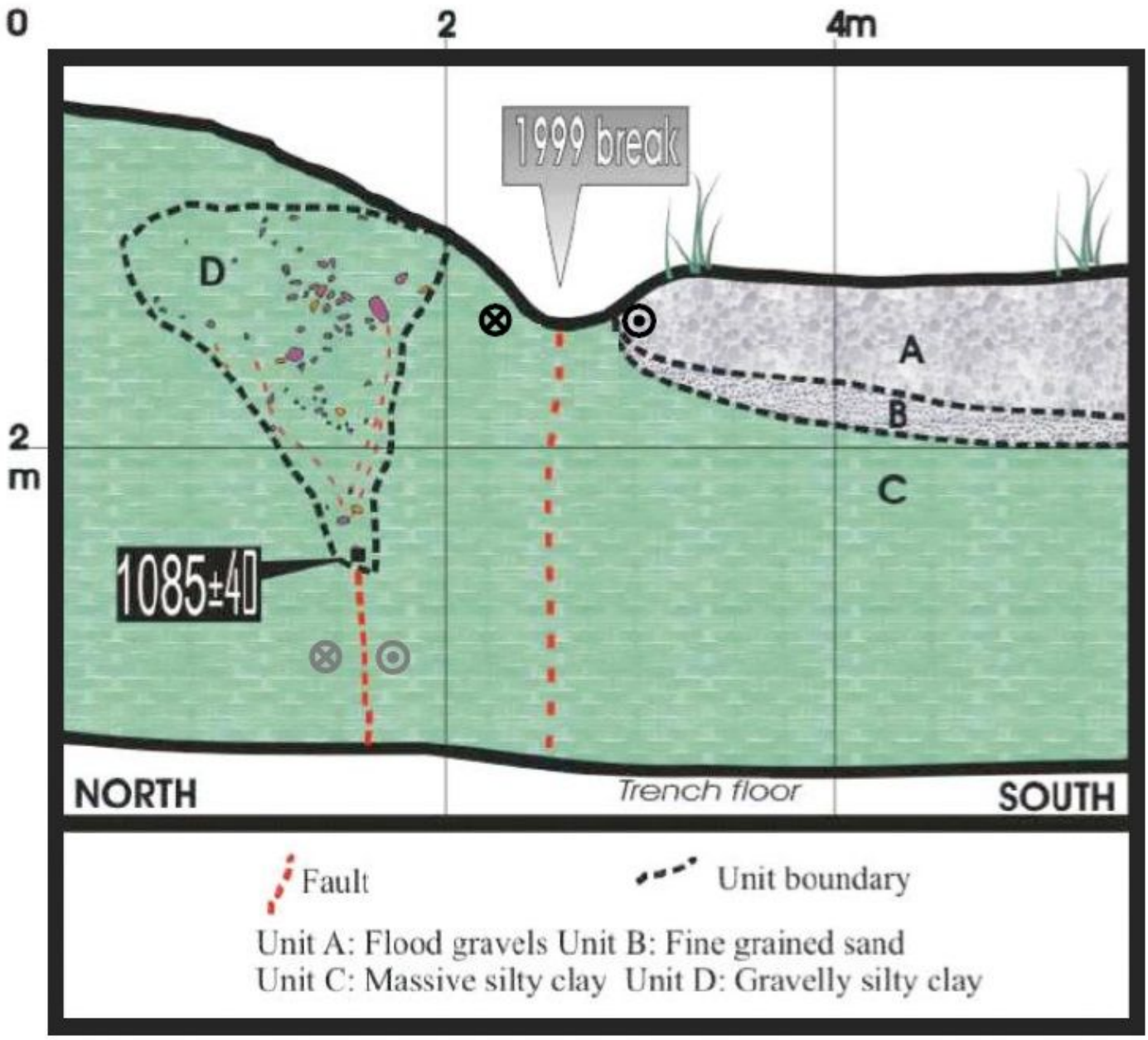

Figure 12

Log of Bend-3 trench. See figure 7 for the trench site. Unit A and B are flood deposits. Location of the 1999 rupture is not clearly detectable in the trench wall due to the unstratified nature of the unit C material. Unit D is a wedge-fill related to event D. It contains gravelly silt deposits. Carbon sample location is outlined in black square at the bottom tip of the wedge (R28325/3). The conventional 14C age for this sample is given in the rectangle (Table 1).

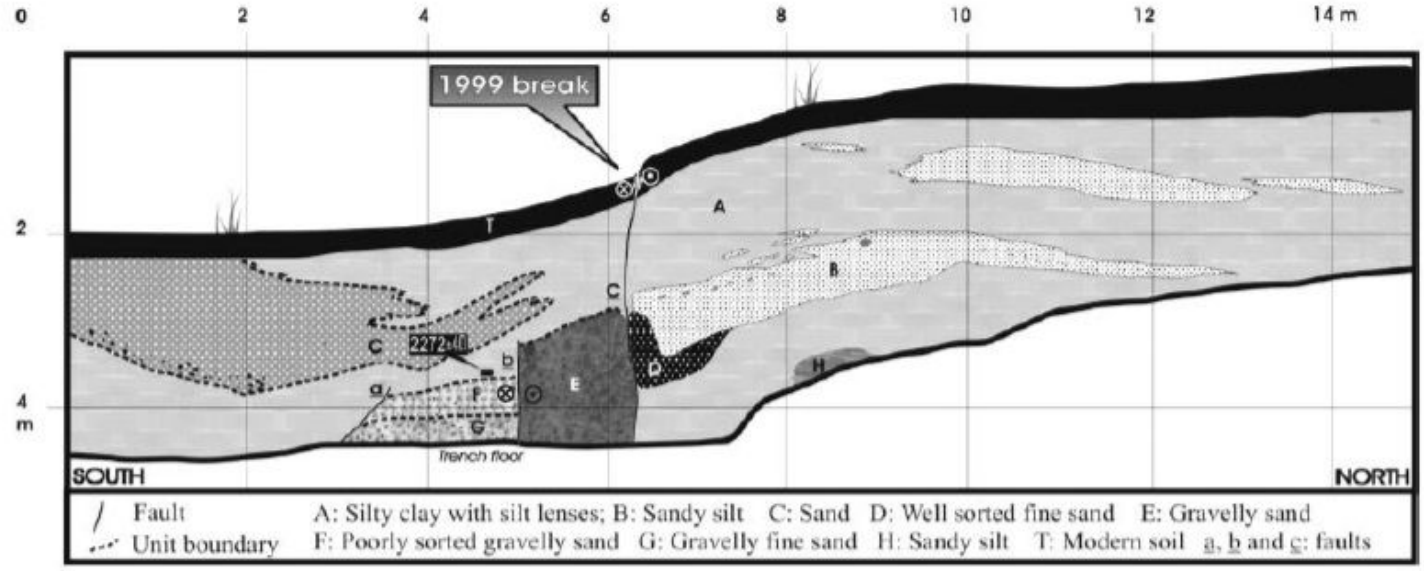

Figure 13

Log of Kaledibi-1 trench. See figure 8 for the trench location. The southern half of the trench is divided into four structural blocks by the faults a, b and c. Fault b is buried by unit C and pre-dated by a sample. The event B is related to this faulting. Location of this carbon sample is outlined in black square (R28325/5). Its conventional 14C age is given in the rectangle (Table 1).

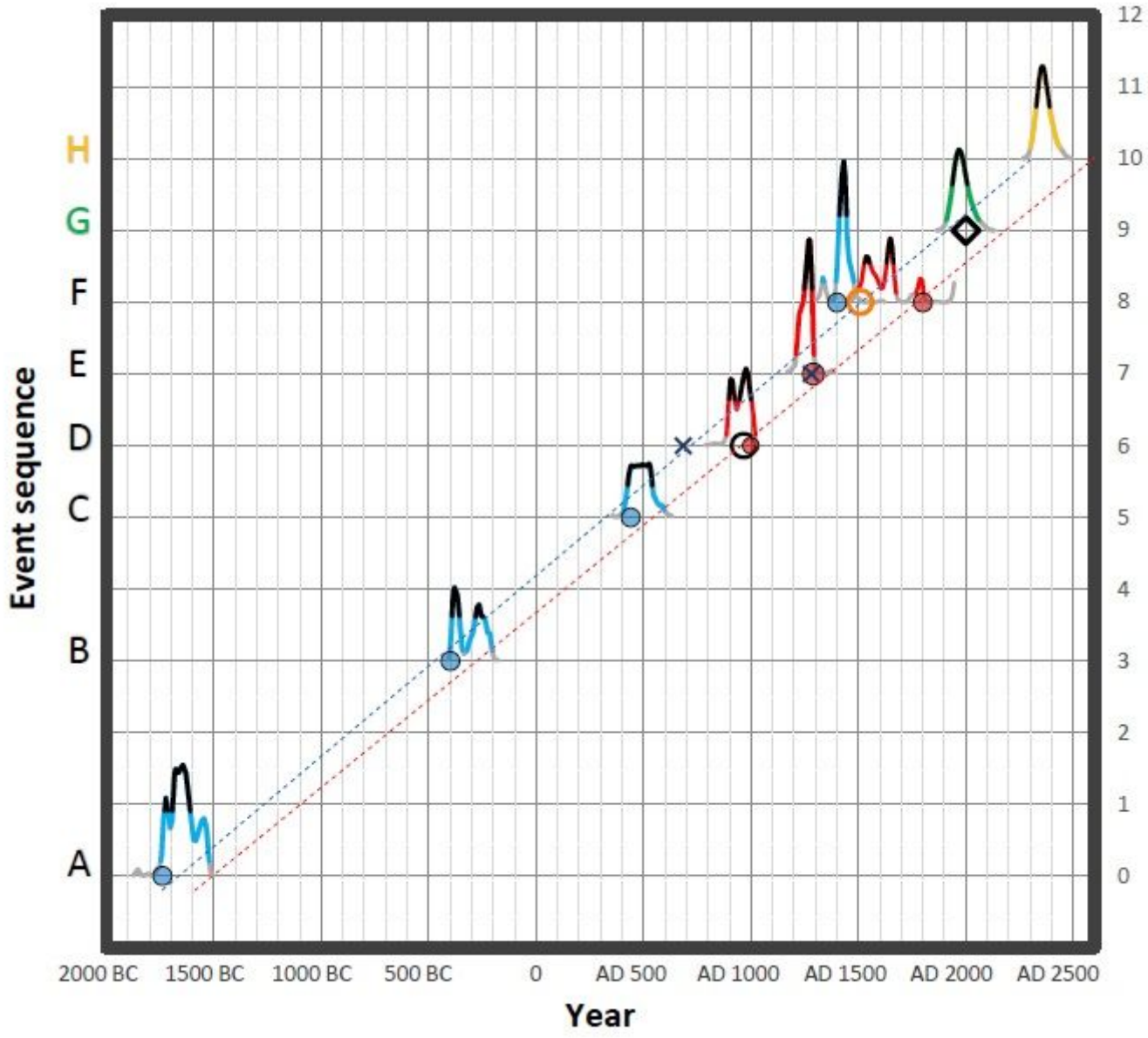

Figure 14

Linear sequential event serial (SES) model. Event name and sequence on left and right vertical axis, respectively. There are seven calibrated radiometric age probability distributions (black 1σ; blue or red 2σ) in 0, 3, 5, 6, 7, 8th event order for events A to F. Blue and red colored distributions represent pre- and post-dates, respectively. Age samples (carbon) were dated (AMS) and calibrated (Bronk Ramsey 1995, 2001, 2004) to RAFTER Radiocarbon Laboratory. Probability distributions (black 68 %; green or yellow 95 %) for 1999 (green) and future (yellow) earthquakes were predicted according to probability distribution-based method (PDBM). Diamond represents November 12, 1999 Düzce earthquake. Black and orange hollow circles are September 2, 967 and September 10, 1509 historical earthquakes, respectively. Blue crosses are AD 1280 and AD 685 pre-dates suggested in Pantosti et al. (2008). They are adaptable to event E and D, respectively. On the other hand, AD 1280 underestimates our minimum value of 68.2 % probability curve of pre- dating sample for event F (Table 1). Blue- and red-filled circles are minimum and maximum limits of 68.2 % region of age probability distributions of pre- and post-date samples, respectively (Table

1). Dashed blue and red lines are linear least square fits for blue- and red-filled circles, respectively. RMS values are 0.98 and 0.99 for fit lines based on post- and pre-dating samples, respectively.

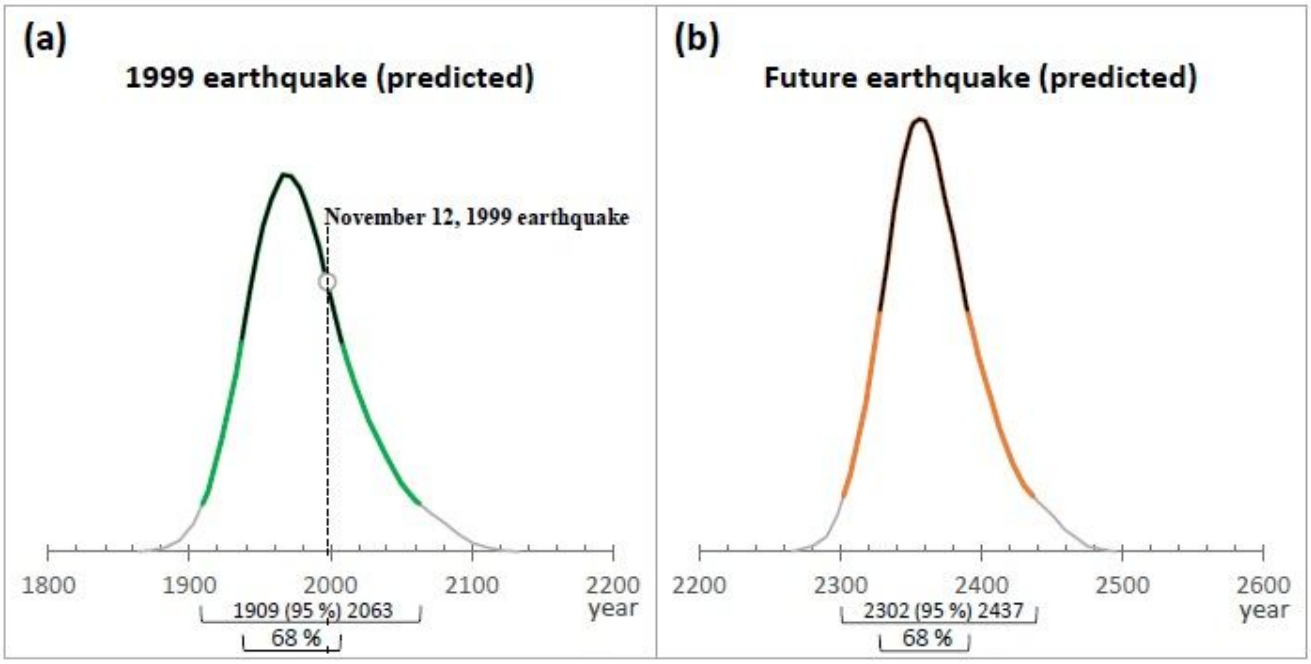

Figure 15

Predicted earthquakes based on probability distribution-based method (PDBM). 1σ region is under the black curve. (a) Probability distribution for 1999 earthquake. It was predicted between 1933 and 2005 with 68 % probability. (a) Probability distribution for future earthquake. It was predicted between 2328 and 2392 with 68 % probability. The earthquake recurrence interval about 391 ± 34 years with % 68 probability for Düzce fault according to the PDBM. Suggested date was 1609 ± 34 with 68 % probability for the penultimate event (event F) according to the PDBM.